Available online at www.sciencedirect.com
ScienceDirect
Journal of Computational Physics 224 (2007) 699–711
JOURNAL OF COMPUTATIONAL PHYSICS
www.elsevier.com/locate/jcp

Spin-polarized currents in ferromagnetic multilayers

Carlos J. García-Cervera [a,*], Xiao-Ping Wang [b]

[a] Mathematics Department, University of California, Santa Barbara, CA 93106, United States
[b] Mathematics Department, Hong Kong University of Science and Technology, Kowloong, Hong Kong

Received 20 March 2006; received in revised form 28 September 2006; accepted 17 October 2006
Available online 8 December 2006

Abstract

We present a semi-implicit numerical method for micromagnetics simulations, in the presence of spin-currents. The dynamics of the magnetization are described by the Landau–Lifshitz–Gilbert equation, while the dynamics of the spin are described by a diffusion equation with discontinuous coefficients. The complexity of the method presented is comparable to that of solving the linear heat equation with the Backward Euler method. To illustrate the procedure, we carry out three dimensional simulations of the magnetization reversal process in a magnetic multilayer when a current flows perpendicular to the layers. Spin-polarized currents are shown to decrease the coercive field, and to induce magnetization reversal even in the absence of external magnetic fields.
© 2006 Elsevier Inc. All rights reserved.

Keywords: Micromagnetics; Spin polarized transfer; Landau–Lifshitz–Gilbert

1. Introduction

Magnetic storage devices rely on the fact that ferromagnetic materials are typically bistable, and that it is possible to switch between different states by applying a magnetic field. The discovery of the Giant Magneto-Resistance effect has enabled the use of layered ferromagnetic materials in magnetic devices, such as magnetic memories (MRAMs). Even in the absence of thermal effects, there are limitations in the storage capacity of such devices due to the fact that as the size is decreased, the magnitude of the switching field increases, due to an increase in shape anisotropy. Given that magnetic fields have long range interactions, the density of such devices is limited.

A new mechanism for magnetization reversal in multilayers was proposed by Slonczweski [1] and Berger [2,3]. In this new mechanism, an electric current flows perpendicular to the layers. The current is polarized in the first layer, and the polarization travels with the current to the second layer, where it interacts with the underlying magnetization. Since currents are localized in each cell, long range effects can be reduced.

* Corresponding author.
E-mail addresses: cgarcia@math.ucsb.edu (C.J. García-Cervera), mawang@ust.hk (X.-P. Wang).
URLs: http://www.math.ucsb.edu/~cgarcia (C.J. García-Cervera), http://www.math.ust.hk/~mawang (X.-P. Wang).

0021-9991/$ - see front matter © 2006 Elsevier Inc. All rights reserved.
doi:10.1016/j.jcp.2006.10.029

In the original model for spin polarized transport, the magnetization was assumed constant, or *pinned*, in one of the layers, and the polarization was added as an extra field in the effective field. In addition, spin diffusion and interfacial effects were neglected. These effects have been found to be important in magnetoresistance experiments with a current perpendicular to the multilayer planes [4–6]. Recently, a new model for the relaxation of the coupled system spin-magnetization has appeared in the literature [7,8]. This model includes spatial variations in both spin and magnetization, and does not assume a priori that the magnetization is pinned in one of the layers.

The dynamics of the spin accumulation are described by the diffusion equation [7]

$$\frac{\partial \mathbf{s}}{\partial t} = -\mathrm{div}\mathbf{J}_s - 2D_0(\mathbf{x})\frac{\mathbf{s}}{\lambda_{sf}^2} - 2D_0(\mathbf{x})\frac{\mathbf{s}\times\mathbf{m}}{\lambda_J^2}, \tag{1}$$

where $\mathbf{s}$ is the spin accumulation, $\mathbf{m}$ is the magnetization, $\mathbf{J}_s$ is the spin current, D_0 is the diffusion coefficient, λ_{sf} is the characteristic length for spin-flip relaxation, and λ_J is related to the electron's mean free path. The spin current is

$$\mathbf{J}_s = \frac{\beta\mu_B}{e}\mathbf{m}\otimes\mathbf{J}_e - 2D_0(\mathbf{x})[\nabla\mathbf{s} - \beta\beta'\mathbf{m}\otimes(\nabla\mathbf{s}\cdot\mathbf{m})], \tag{2}$$

where $\mathbf{J}_e$ is the applied electric current, $\mu_B = 9.2741\times10^{-24}\ \mathrm{Am}^2$ is the Bohr magneton, $e = -1.602\times10^{-19}$ As is the charge of the electron, and $0<\beta<1$ and $0<\beta'<1$ are (dimensionless) spin-polarization parameters for the magnetic layers. The diffusion coefficient D_0 is discontinuous at the interface, but otherwise is positive and bounded. Eq. (1) results from considering the transport in a multilayer as a diffusive process [8]. The last term in (1) represents the interaction between the spin accumulation and the background magnetization, and is responsible for the transfer of angular momentum between them.

The magnetization is zero outside the magnetic samples, and the spin current is continuous across the ferromagnetic-nonmagnetic interface [9]. As a consequence, the normal derivative of $\mathbf{s}$ is discontinuous at the interface, and therefore standard second order differences do not produce good results in this context.

The relaxation process of the magnetization inside the ferromagnetic samples is described by the Landau–Lifshitz–Gilbert (LLG) equation [10,11]:

$$\frac{\partial \mathbf{m}}{\partial t} = -\gamma\mathbf{m}\times(\mathbf{h}_e + c\mathbf{s}) + \alpha\mathbf{m}\times\frac{\partial\mathbf{m}}{\partial t}. \tag{3}$$

In (3), $\gamma = 1.76\times10^{11}\ (\mathrm{Ts})^{-1}$ is the gyromagnetic ratio, c represents the strength of the interaction between the spin and the magnetization, and α is the dimensionless damping parameter. Given that the length of the magnetization is preserved by Eq. (3), we have normalized the magnetization so that $|\mathbf{m}| = 1$. The first term in (3) describes a precession around the local field $\mathbf{h}_e + c\mathbf{s}$, while the second term accounts for dissipation in the system. The effective field, $\mathbf{h}_e$, is defined as

$$\mathbf{h}_e = -\frac{2K_u}{M_s}(m_2\mathbf{e}_2 + m_3\mathbf{e}_3) + \frac{2C_{ex}}{M_s}\Delta\mathbf{m} + \mu_0(\mathbf{h}_s + \mathbf{h}_0), \tag{4}$$

where we have used $\mathbf{e}_2 = (0,1,0)$, and $\mathbf{e}_3 = (0,0,1)$. In (4), $\mu_0 = 4\pi\times\ 10^{-7}\mathrm{N/A}^2$ is the permeability of vacuum, and M_s is the saturation magnetization. The first and second terms on the right hand side of (4) are the anisotropy and exchange fields, respectively, with K_u and C_{ex} being material constants. $\mathbf{h}_0$ is the externally applied magnetic field.

The stray field, $\mathbf{h}_s = -\nabla u$ is obtained by solving the magnetostatic equation:

$$\begin{aligned} &\Delta u = \mathrm{div}\ \mathbf{m}, \quad \mathbf{x}\in\Omega \\ &\Delta u = 0, \quad \mathbf{x}\in\overline{\Omega}^c \end{aligned} \tag{5}$$

with jump boundary conditions

$$\begin{aligned} &[u]_{\partial\Omega} = 0, \\ &\left[\frac{\partial u}{\partial v}\right]_{\partial\Omega} = -\mathbf{m}\cdot v, \end{aligned} \tag{6}$$

where Ω is the volume occupied by the ferromagnetic samples, and $[\cdot]$ represents the jump at the material/vacuum interface. The solution to this equation is

$$u(\mathbf{x}) = \int_{\Omega} \nabla N(\mathbf{x}-\mathbf{y}) \cdot \mathbf{m}(\mathbf{y})\, d\mathbf{y}, \tag{7}$$

where Ω is the volume occupied by the ferromagnetic sample, and $N(\mathbf{x}) = -1/(4\pi|\mathbf{x}|)$ is the Newtonian potential.

In realistic micromagnetics simulations of the LLG (3), it is necessary to resolve a wide range of spatial length scales, and in particular magnetic walls and magnetic vortices, since these are responsible for the switching anomalies observed experimentally [12,13]. High order accuracy can be obtained with explicit numerical schemes, such as the Runge–Kutta and predictor–corrector schemes [14]. Numerical methods that preserve some of the geometric properties of the equations have also been implemented [15,16]. However, the time step size in these methods is severely constrained by the stability of the numerical scheme. For physical constants characteristic of the permalloy ($M_s = 8.0 \times 10^5$ A/m, $K_u = 5.0 \times 10^2$ J/m^3, $A = 1.3 \times 10^{-11}$ J/m, $\gamma = 1.76 \times 10^{11}$ T^{-1} s^{-1}), with a cell size $\Delta x = 0.004$ μm (256 grid points in a 1 μm long sample), and using fourth order Runge–Kutta, a time step roughly of the order $\Delta t \approx .25$ ps is necessary for numerical stability. If the cell size is decreased by a factor of 10, the time step Δt must be reduced by a factor of 100.

In order to overcome the stability constraint of explicit schemes, one usually resorts to implicit schemes [17]. However, due to the strong nonlinearities present in both the gyromagnetic and damping terms in the LLG Eq. (3), a direct implicit discretization of the system is not efficient and is difficult to implement. The Gauss–Seidel projection method (GSPM) [18,19] is an efficient implicit numerical scheme for the LLG Eq. (3). Only linear systems of equations are solved, and the nonlinearity is introduced *a posteriori*. The method is unconditionally stable, and the complexity is comparable to that of solving the linear heat equation using the Backward Euler method.

In this article we develop an unconditionally stable numerical method for a three dimensional version of the model presented in [7]. A splitting procedure is derived for the spin equation (1), which is subsequently combined with the GSPM for the LLG.

The remainder of this article is organized as follows: In Section 2 we describe a second order accurate spatial discretization, and we explain how this can be used with both explicit and implicit time evolution schemes. An implicit scheme based on splitting of Eq. (1) is presented in Section 3. Finally, we use this method to simulate the magnetization reversal process in a multilayer in the presence of spin-polarized currents.

2. Spatial discretization

We consider a rectangular multilayer consisting of two ferromagnetic layers (FM1 and FM2) of thickness D_1 and D_3, respectively, separated by a non-magnetic layer (NM) of thickness D_2 (see Fig. 1). We only con-

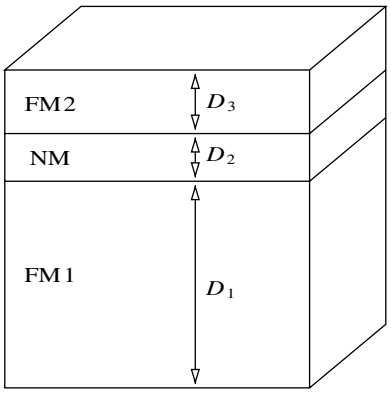

Fig. 1. Structure of the multilayer: Two ferromagnetic layers (FM1 and FM2) of thickness D_1 and D_3, respectively, separated by a non-magnetic layer (NM) of thickness D_2.

sider here the case of a straight interface. The methodology presented here can be combined with the ideas presented in [20] when arbitrarily shaped samples are considered. The domain is discretized using a uniform mesh. The magnetization and the spin accumulation are defined at the center of the computational cells. The spin current must be continuous at the interface between the ferromagnetic and non-magnetic materials:

$$-2D_0^{\text{out}}\frac{\partial \mathbf{s}^{\text{out}}}{\partial z} = \frac{\beta j_e \mu_B}{e}\mathbf{m} - 2D_0^{\text{in}}\left[\frac{\partial \mathbf{s}^{\text{in}}}{\partial z} - \beta\beta'\left(\mathbf{m}, \frac{\partial \mathbf{s}^{\text{in}}}{\partial z}\right)\mathbf{m}\right], \tag{8}$$

where we indicate by *in* and *out* the values of $\mathbf{s}$ and D_0 inside and outside of the ferromagnetic layer, respectively.

Consider the situation described in Fig. 2. The value $\mathbf{s}_0$ is an auxiliary value needed to impose the interface condition (8), and to compute the second derivatives of the spin accumulation near the interface. To do this, we construct interpolating polynomials in the interior and the exterior of the ferromagnetic layers. The interior polynomial is defined by the values $\mathbf{s}_0$, $\mathbf{s}_{-1}$, $\mathbf{s}_{-2}$, and $\mathbf{s}_{-3}$. The exterior polynomial is defined by $\mathbf{s}_0$, $\mathbf{s}_1$, $\mathbf{s}_2$, and $\mathbf{s}_3$.

The value of $\mathbf{m}$ at the interface can be evaluated either via extrapolation from interior values,

$$\mathbf{m}_0 = \frac{3\mathbf{m}_{-1} - \mathbf{m}_{-2}}{2} + O(\Delta z^2) \tag{9}$$

or taking into account that $\frac{\partial \mathbf{m}}{\partial z} = 0$, so

$$\mathbf{m}_0 = \mathbf{m}_{-1} + O(\Delta z^2). \tag{10}$$

The value of $\mathbf{s}_0$ may be determined (in terms of $\mathbf{s}_{-3}$, $\mathbf{s}_{-2}$, $\mathbf{s}_{-1}$, $\mathbf{s}_1$, $\mathbf{s}_2$, and $\mathbf{s}_3$) by imposing condition (8) to the interior and exterior polynomials. The second derivatives of $\mathbf{s}$ near the interface are approximated by the second derivatives of the corresponding polynomials.

2.1. Explicit time-stepping

To illustrate how to use this approach in combination with an explicit time-stepping procedure, consider the following interpolating polynomials in the interior,

$$p_{\text{in}}(z) = \mathbf{s}_{-3} + \frac{\mathbf{s}_{-2} - \mathbf{s}_{-3}}{\Delta z}(z - z_{-3}) + \frac{\mathbf{s}_{-1} - 2\mathbf{s}_{-2} + \mathbf{s}_{-3}}{2\Delta z^2}(z - z_{-3})(z - z_{-2}) + \frac{8\mathbf{s}_0 - 15\mathbf{s}_{-1} + 10\mathbf{s}_{-2} - 3\mathbf{s}_{-3}}{15\Delta z^3}(z - z_{-3})(z - z_{-2})(z - z_{-1}), \tag{11}$$

and in the exterior:

$$p_{\text{out}}(z) = \mathbf{s}_3 - \frac{\mathbf{s}_2 - \mathbf{s}_3}{\Delta z}(z - z_3) + \frac{\mathbf{s}_1 - 2\mathbf{s}_2 + \mathbf{s}_3}{2\Delta z^2}(z - z_3)(z - z_2) - \frac{8\mathbf{s}_0 - 15\mathbf{s}_1 + 10\mathbf{s}_2 - 3\mathbf{s}_3}{15\Delta z^3}(z - z_3)(z - z_2)(z - z_1). \tag{12}$$

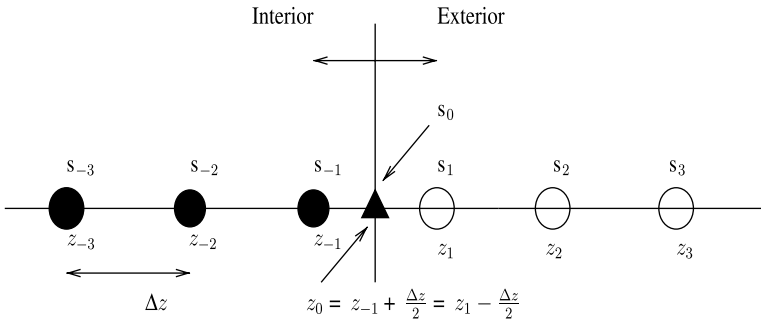

Fig. 2. Discretization nodes and approximation of the second derivative at the ferromagnetic/non-magnetic interface. The figure is rotated so that the Z-axis looks horizontal.

Using these formulas, we get, at the first interface:

$$p'_{\text{in}}(z_0) = \frac{184\mathbf{s}_0 - 225\mathbf{s}_{-1} + 50\mathbf{s}_{-2} - 9\mathbf{s}_{-3}}{60\Delta z}$$
$$p''_{\text{in}}(z_{-1}) = \frac{16\mathbf{s}_0 - 25\mathbf{s}_{-1} + 10\mathbf{s}_{-2} - \mathbf{s}_{-3}}{5\Delta z^2}, \tag{13}$$

and

$$p'_{\text{out}}(z_0) = \frac{-184\mathbf{s}_0 + 225\mathbf{s}_1 - 50\mathbf{s}_2 + 9\mathbf{s}_3}{60\Delta z}$$
$$p''_{\text{out}}(z_1) = \frac{16\mathbf{s}_0 - 25\mathbf{s}_1 + 10\mathbf{s}_2 - \mathbf{s}_3}{5\Delta z^2}. \tag{14}$$

Substituting in (8), we get:

$$-2D_0^{\text{out}}\frac{-184\mathbf{s}_0 + 225\mathbf{s}_1 - 50\mathbf{s}_2 + 9\mathbf{s}_3}{60\Delta z} = -\frac{\beta j_e \mu_B}{e}\mathbf{m}_0 - 2D_0^{\text{in}}\left[\frac{184\mathbf{s}_0 - 225\mathbf{s}_{-1} + 50\mathbf{s}_{-2} - 9\mathbf{s}_{-3}}{60\Delta z} - \beta\beta'\left(\mathbf{m}_0, \frac{184\mathbf{s}_0 - 225\mathbf{s}_{-1} + 50\mathbf{s}_{-2} - 9\mathbf{s}_{-3}}{60\Delta z}\right)\mathbf{m}_0\right] \tag{15}$$

Taking the inner product with $\mathbf{m}_0$,

$$(\mathbf{s}_0, \mathbf{m}_0) = \frac{5\Delta z(\mathbf{f}, \mathbf{m}_0)}{24(D_0^{\text{out}} + D_0^{\text{in}} - D_0^{\text{in}}\beta\beta'|\mathbf{m}_0|^2)}, \tag{16}$$

where

$$\mathbf{f} = 2D_0^{\text{out}}\frac{225\mathbf{s}_1 - 50\mathbf{s}_2 + 9\mathbf{s}_3}{60\Delta z} - \frac{\beta j_e \mu_B}{e}\mathbf{m}_0 - 2D_0^{\text{in}}\left[\frac{-225\mathbf{s}_{-1} + 50\mathbf{s}_{-2} - 9\mathbf{s}_{-3}}{60\Delta z} - \beta\beta'\left(\mathbf{m}_0, \frac{-225\mathbf{s}_{-1} + 50\mathbf{s}_{-2} - 9\mathbf{s}_{-3}}{60\Delta z}\right)\mathbf{m}_0\right]. \tag{17}$$

Once $(\mathbf{s}_0, \mathbf{m}_0)$ is known, $\mathbf{s}_0$ can be determined from (15):

$$\mathbf{s}_0 = \frac{5\Delta z}{24(D_0^{\text{out}} + D_0^{\text{in}})}\left(\frac{24D_0^{\text{in}}}{5\Delta z}(\mathbf{m}_0, \mathbf{s}_0) + \mathbf{f}\right). \tag{18}$$

This value of $\mathbf{s}_0$ can be used in formulas (11) and (12) to approximate the derivatives of $\mathbf{s}$ near the interface to second order accuracy. An analogous procedure needs to be carried out at the second interface. Once the value of $\mathbf{s}_0$ is known, the right hand side of (1) can be evaluated at time t_n using formulas (13) and (14), and an explicit time stepping procedure such as the fourth order Runge–Kutta method can be used to advance in time.

2.2. Implicit time-stepping

The procedure described above can be used with an implicit time step as well. The resulting system of equations is still linear, but it has non-constant coefficients. We can obtain a linear system of equations with constant coefficients if the following condition is imposed at the interface:

$$-2D_0^{\text{out}}\frac{-184\mathbf{s}_0^{n+1} + 225\mathbf{s}_1^{n+1} - 50\mathbf{s}_2^{n+1} + 9\mathbf{s}_3^{n+1}}{60\Delta z} = -\frac{\beta j_e \mu_B}{e}\mathbf{m}_0^n - 2D_0^{\text{in}}\left[\frac{184\mathbf{s}_0^{n+1} - 225\mathbf{s}_{-1}^{n+1} + 50\mathbf{s}_{-2}^{n+1} - 9\mathbf{s}_{-3}^{n+1}}{60\Delta z} - \beta\beta'\left(\mathbf{m}_0^n, \frac{184\mathbf{s}_0^n - 225\mathbf{s}_{-1}^n + 50\mathbf{s}_{-2}^n - 9\mathbf{s}_{-3}^n}{60\Delta z}\right)\mathbf{m}_0^n\right]. \tag{19}$$

In (19) we denote with the superscripts n and $n+1$ the values of $\mathbf{s}$ at times t_n and t_{n+1}, respectively. The linear terms are treated implicitly, and the nonlinear terms explicitly. Since $0 < \beta < 1$ and $|\mathbf{m}| = 1$, the stability of the method is not affected by the explicit treatment of the nonlinear terms in the higher derivatives. This choice also allows us to solve only linear systems of equations with constant coefficients. Then,

$$\mathbf{s}_0^{n+1} = \frac{5\Delta z}{24(D_0^{\text{out}} + D_0^{\text{in}})}\left(-\frac{\beta j_e \mu_B}{e}\mathbf{m}_0^n + 2D_0^{\text{out}}\frac{225\mathbf{s}_1^{n+1} - 50\mathbf{s}_2^{n+1} + 9\mathbf{s}_3^{n+1}}{60\Delta z} - 2D_0^{\text{in}}\left[\frac{-225\mathbf{s}_{-1}^{n+1} + 50\mathbf{s}_{-2}^{n+1} - 9\mathbf{s}_{-3}^{n+1}}{60\Delta z} - \beta\beta'\left(\mathbf{m}_0^n, \frac{184\mathbf{s}_0^n - 225\mathbf{s}_{-1}^n + 50\mathbf{s}_{-2}^n - 9\mathbf{s}_{-3}^n}{60\Delta z}\right)\mathbf{m}_0^n\right]\right). \tag{20}$$

Using this and (11) and (12), we obtain

$$2D_0^{\text{in}}\frac{\partial^2 \mathbf{s}}{\partial z^2}(\mathbf{z}_{-1}) \approx \frac{2D_0^{\text{in}}}{5\Delta z^2}\left\{\frac{10}{3(D_0^{\text{out}} + D_0^{\text{in}})}\left(-\frac{\beta j_e \mu_B \Delta z}{e}\mathbf{m}_0^n + \frac{D_0^{\text{out}}}{30}(225\mathbf{s}_1^{n+1} - 50\mathbf{s}_2^{n+1} + 9\mathbf{s}_3^{n+1}) - \frac{D_0^{\text{in}}}{30}\left[(-225\mathbf{s}_{-1}^{n+1} + 50\mathbf{s}_{-2}^{n+1} - 9\mathbf{s}_{-3}^{n+1}) - \beta\beta'\left(\mathbf{m}_0^n, 184\mathbf{s}_0^n - 225\mathbf{s}_{-1}^n + 50\mathbf{s}_{-2}^n - 9\mathbf{s}_{-3}^n\right)\mathbf{m}_0^n\right]\right) - 25\mathbf{s}_{-1}^{n+1} + 10\mathbf{s}_{-2}^{n+1} - \mathbf{s}_{-3}^{n+1}\right\}, \tag{21}$$

and

$$2D_0^{\text{out}}\frac{\partial^2 \mathbf{s}}{\partial z^2}(\mathbf{z}_1) \approx \frac{2D_0^{\text{out}}}{5\Delta z^2}\left\{\frac{10}{3(D_0^{\text{out}} + D_0^{\text{in}})}\left(-\frac{\beta j_e \mu_B \Delta z}{e}\mathbf{m}_0^n + \frac{D_0^{\text{out}}}{30}(225\mathbf{s}_1^{n+1} - 50\mathbf{s}_2^{n+1} + 9\mathbf{s}_3^{n+1}) - \frac{D_0^{\text{in}}}{30}\left[(-225\mathbf{s}_{-1}^{n+1} + 50\mathbf{s}_{-2}^{n+1} - 9\mathbf{s}_{-3}^{n+1}) - \beta\beta'\left(\mathbf{m}_0^n, 184\mathbf{s}_0^n - 225\mathbf{s}_{-1}^n + 50\mathbf{s}_{-2}^n - 9\mathbf{s}_{-3}^n\right)\mathbf{m}_0^n\right]\right) - 25\mathbf{s}_1^{n+1} + 10\mathbf{s}_2^{n+1} - \mathbf{s}_3^{n+1}\right\}. \tag{22}$$

3. Temporal discretization: splitting algorithm

Stability issues require that an implicit scheme be used for the coupled system spin/magnetization, Eqs. (1) and (3). We present here an unconditionally stable method for this coupled system based on a splitting of Eq. (1). This splitting procedure is coupled to the GSPM for the Landau-Lifshitz equation [18,19].

To illustrate the procedure, we consider the following simplified one-dimensional case:

$$\begin{aligned}\frac{\partial \mathbf{s}}{\partial t} &= \frac{\partial}{\partial z}\left(a(z)\left(\frac{\partial \mathbf{s}}{\partial z} - \beta\left(\mathbf{m}, \frac{\partial \mathbf{s}}{\partial z}\right)\mathbf{m}\right)\right) - a(z)\mathbf{s} - a(z)\mathbf{s}\times\mathbf{m} - \frac{\partial \mathbf{m}}{\partial z},\\ \frac{\partial \mathbf{m}}{\partial t} &= -\mathbf{m}\times\left(\frac{\partial^2 \mathbf{m}}{\partial z^2} + \mathbf{s}\right) + \alpha\mathbf{m}\times\frac{\partial \mathbf{m}}{\partial t},\end{aligned} \tag{23}$$

$$a(z) = \begin{cases} a_{\text{in}} & \text{inside the ferromagnetic sample,}\\ a_{\text{out}} & \text{outside the ferromagnetic sample.}\end{cases} \tag{24}$$

Given $\mathbf{m}^n = \mathbf{m}(t_n)$ and $\mathbf{s}^n = \mathbf{s}(t_n)$, the numerical method proceeds in three steps:

Step I. Solve the Cauchy problem

$$\begin{aligned}\frac{d\widetilde{\mathbf{s}}}{dt} &= -a(z)\widetilde{\mathbf{s}} - a(z)\widetilde{\mathbf{s}}\times\mathbf{m}^n,\\ \widetilde{\mathbf{s}}(t_n) &= \mathbf{s}^n.\end{aligned} \tag{25}$$

The solution to this problem can be found analytically, and is given in Lemma (1) below.

Step II. Solve the following system of equations:

$$\frac{\mathbf{s}^{n+1} - \widetilde{\mathbf{s}}(t_{n+1})}{\Delta t} = a(z)\widetilde{D_z}^2\mathbf{s}^{n+1} - \beta a(z)D_z((\mathbf{m}, D_z\mathbf{s}^n)\mathbf{m}^n) - D_z\mathbf{m}^n. \tag{26}$$

The operator D_z denotes the approximation to the first derivative using standard second order differences (centered in the interior of the domain, and one-sided near the endpoints). $\widetilde{D_z}^2$ represents

the approximation to the second derivative that uses standard centered differences away from the interface, and next to the interface is given by (21) and (22). The resulting system is heptadiagonal, and can be solved using Gauss elimination in O(N) operations.

Step III. Solve equation

$$\frac{\partial \mathbf{m}}{\partial t} = -\mathbf{m} \times \left(\frac{\partial^2 \mathbf{m}}{\partial z^2} + \mathbf{s}^{n+1} \right) + \alpha \mathbf{m} \times \frac{\partial \mathbf{m}}{\partial t},$$
$$\mathbf{m}(t_n, z) = \mathbf{m}^n,$$

from t_n to t_{n+1} using the GSPM [18].

The GSPM is a semi-implicit method for the LLG equation based on a splitting of Eq. (3). Only linear systems of equations are solved, and the nonlinearity is added *a posteriori*. Therefore, the complexity of the splitting algorithm is comparable to that of solving the linear heat equation using the Backward Euler method. For completeness, a description of the GSPM is included in Appendix A. For further details, see [18,19].

The following lemma has been used in Step I:

Lemma 1. *Consider the following ordinary differential equation*:

$$\frac{d\mathbf{w}}{d\tau} = -a\mathbf{w} - b\mathbf{w} \times \mathbf{m}, \tag{27}$$

where $a, b \in \mathbb{R}$, *and* $\mathbf{m} \in \mathbb{R}^3$ *are constants. The solution to* (27) *with initial condition* $\mathbf{w}(\tau_0) = \mathbf{w}_0$ *is*

$$\mathbf{w}(\tau) = \mathbf{e}^{-a(\tau-\tau_0)} \mathbf{R}^{\mathrm{T}} \cdot \begin{pmatrix} 1 & 0 & 0 \\ 0 & \cos(b(\tau-\tau_0)) & -\sin(b(\tau-\tau_0)) \\ 0 & \sin(b(\tau-\tau_0)) & \cos(b(\tau-\tau_0)) \end{pmatrix} \cdot \mathbf{R} \cdot \mathbf{w}_0, \tag{28}$$

where

$$\mathbf{R} = \begin{pmatrix} m_1 & m_2 & m_3 \\ 0 & \frac{m_3}{\sqrt{m_2^2+m_3^2}} & -\frac{m_2}{\sqrt{m_2^2+m_3^2}} \\ -\sqrt{m_2^2+m_3^2} & \frac{m_1 m_2}{\sqrt{m_2^2+m_3^2}} & \frac{m_1 m_3}{\sqrt{m_2^2+m_3^2}} \end{pmatrix} \tag{29}$$

satisfies $\mathbf{R}^{\mathrm{T}} \cdot \mathbf{R} = \mathbf{R}^{\mathrm{T}} \cdot \mathbf{R}^{\mathrm{T}} = \mathbf{I}$, $\mathbf{R} \cdot \mathbf{m} = \mathbf{e}_1$, *and* $\det(\mathbf{R}) = 1$.

Remark 2. The matrix $\mathbf{R}$ can be obtained as a product of Givens rotations, and therefore it is an orthogonal matrix.

Remark 3. If $m_2 = m_3 = 0$, we define

$$\mathbf{R} = \begin{pmatrix} m_1 & 0 & 0 \\ 0 & 1 & 0 \\ 0 & 0 & m_1 \end{pmatrix} \tag{30}$$

Proof of Lemma 1. Define $\mathbf{q} = \mathbf{e}^{a(\tau-\tau_0)}\mathbf{w}$. Then $\mathbf{q}(\tau_0) = \mathbf{w}(\tau_0)$, and $\mathbf{q}$ satisfies the equation

$$\frac{d\mathbf{q}}{d\tau} = -b\mathbf{q} \times \mathbf{m}. \tag{31}$$

Since $\mathbf{m} = \mathbf{R}^{\mathrm{T}} \cdot \mathbf{e}_1$, we get

$$\frac{d\mathbf{q}}{d\tau} = -b\mathbf{R}^{\mathrm{T}} \cdot ((\mathbf{R} \cdot \mathbf{q}) \times \mathbf{e}_1). \tag{32}$$

Therefore, $\mathbf{v} = \mathbf{R} \cdot \mathbf{q}$ satisfies equation

$$\frac{d\mathbf{v}}{d\tau} = -b\mathbf{v} \times \mathbf{e}_1, \tag{33}$$

with initial value $\mathbf{v}(\tau_0) = \mathbf{R} \cdot \mathbf{w}_0$. The solution to this initial value problem is

$$\mathbf{v}(\tau) = \begin{pmatrix} 1 & 0 & 0 \\ 0 & \cos(b(\tau - \tau_0)) & -\sin(b(\tau - \tau_0)) \\ 0 & \sin(b(\tau - \tau_0)) & \cos(b(\tau - \tau_0)) \end{pmatrix} \cdot \mathbf{R} \cdot \mathbf{w}_0. \tag{34}$$

The proof concludes by undoing the changes, and rewriting (34) is terms of $\mathbf{w}$. □

3.1. Accuracy check: exact solutions

To check the performance of the splitting method described in Section 3, we consider the forced system

$$\begin{aligned} \frac{\partial \mathbf{s}}{\partial t} &= \frac{\partial}{\partial z}\left(a(z)\left(\frac{\partial \mathbf{s}}{\partial z} - \beta\left(\mathbf{m}, \frac{\partial \mathbf{s}}{\partial z}\right)\mathbf{m}\right)\right) - a(z)\mathbf{s} - a(z)\mathbf{s} \times \mathbf{m} - \frac{\partial \mathbf{m}}{\partial z} + \mathbf{g}, \\ \frac{\partial \mathbf{m}}{\partial t} &= -\mathbf{m} \times \left(\frac{\partial^2 \mathbf{m}}{\partial z^2} + \mathbf{s} + \mathbf{f}\right) + \alpha \mathbf{m} \times \frac{\partial \mathbf{m}}{\partial t}, \end{aligned} \tag{35}$$

for $z \in [0,D]$, where $D = D_1 + D_2 + D_3$, with boundary conditions

$$\begin{aligned} &\frac{\partial \mathbf{s}}{\partial z} = 0, \quad z = 0, D, \\ &\frac{\partial \mathbf{m}}{\partial z} = 0, \quad z = 0, D_1, D_1 + D_2, D. \end{aligned} \tag{36}$$

We have chosen $D_1 = D_3 = 0.8$, and $D_2 = 0.4$. The diffusion coefficient takes the values $a^{\text{in}} = 2$, and $a^{\text{out}} = 1$.

We consider a solution of the form $\mathbf{m} = (\cos\theta\cos\psi,\ \cos\theta\sin\psi,\ \sin\theta)$, where

$$\begin{aligned} \theta(z) &= \cos(t)\cos(\pi z/D_1), \\ \psi(z) &= \cos(2t)\cos(3\pi z/D_1), \end{aligned} \tag{37}$$

in FM1, and

$$\begin{aligned} \theta(z) &= \cos(t)\cos(\pi(z - D_1 - D_2)/D_3), \\ \psi(z) &= \cos(2t)\cos(3\pi(z - D_1 - D_2)/D_3), \end{aligned} \tag{38}$$

in FM2. We also define

$$\mathbf{s}^{\text{in}}(t,z) = \sin(t)\begin{pmatrix} \cos(\pi z/D) \\ \sin(\pi(z/D - 1/2)) \\ \cos(3\pi z/D) \end{pmatrix}, \tag{39}$$

inside the ferromagnetic layers $FM1 \cup FM2$.

In the non-magnetic layer, we define

$$\mathbf{s}^{\text{out}}(t,z) = \mathbf{a}(t)\sinh(z - D_1) + \mathbf{b}(t)\cosh(z - D_1) + \mathbf{c}(t)(z - D_1) + \mathbf{d}(t), \tag{40}$$

where $\mathbf{a}, \mathbf{b}, \mathbf{c}, \mathbf{d} \in \mathbb{R}^3$ are determined by imposing the interface conditions:

$$\begin{aligned} &\mathbf{s}^{\text{in}} = \mathbf{s}^{\text{out}}, \\ &a_{\text{out}}\frac{\partial \mathbf{s}^{\text{out}}}{\partial z} = a_{\text{in}}\left[\frac{\partial \mathbf{s}^{\text{in}}}{\partial z} - \beta\left(\frac{\partial \mathbf{s}^{\text{in}}}{\partial z}, \mathbf{m}\right)\mathbf{m}\right] - \mathbf{m}, \end{aligned} \tag{41}$$

at $z = D_1$ and $z = D_1 + D_2$.

Table 1
Error in the solution (**m**,**s**) at time $t = 1$ for different time steps

Temporal accuracy				
Δt	L_∞-error in $\mathbf{m}_1$	L_∞-error in $\mathbf{m}_2$	L_∞-error in $\mathbf{s}$	Order
10^{-1}	1.0931×10^{-2}	5.6534×10^{-2}	5.5155×10^{-2}	
$10^{-1}/2$	5.5623×10^{-3}	3.1745×10^{-2}	2.2965×10^{-2}	1.02378
$10^{-1}/4$	2.7993×10^{-3}	1.7308×10^{-2}	1.0419×10^{-2}	1.00198
$10^{-1}/8$	1.3997×10^{-3}	9.1363×10^{-3}	4.94153×10^{-3}	0.99930

The error is measured in the sup-norm. We use $\Delta z = D/128$. The splitting method presented is first order in time.

Table 2
Error in the solution (**m**,**s**) at time $t = 1$ for different spatial resolutions

Spatial accuracy				
Δz	L_∞-error in $\mathbf{m}_1$	L_∞-error in $\mathbf{m}_2$	L_∞-error in $\mathbf{s}$	Order
6.2500×10^{-3}	5.1971×10^{-2}	6.5927×10^{-2}	7.6697×10^{-2}	
3.1250×10^{-3}	1.1191×10^{-2}	1.4404×10^{-2}	1.7294×10^{-2}	2.18621
1.5625×10^{-3}	2.7992×10^{-3}	3.6119×10^{-3}	4.3678×10^{-3}	1.99340
7.8125×10^{-4}	6.9534×10^{-4}	8.9778×10^{-4}	1.0842×10^{-3}	2.00931

The error is measured in the sup-norm. The time step is fixed at $\Delta t = 10^{-6}$. The method is globally second order accurate in space.

The forcing **g** and **f** was chosen such that the functions **m** and **s** defined above are in fact solutions to system (35).

The errors for different spatio-temporal resolutions are shown in Tables 1 and 2. The errors are computed in the L_∞-norm. It follows from these results that the method is first order accurate in time. In addition, full second order spatial accuracy is recovered, even near the interface.

4. Magnetization reversal in multilayers

We have used this method to carry out fully resolved three dimensional simulations of the magnetization reversal process in a nanometer sized multilayer, using equations (1)–(7). For the ferromagnetic layers, we have used physical constants characteristic of the Permalloy: $M_s = 8.0 \times 10^5$ A/m, $K_u = 5.0 \times 10^2$ J/m^3, and $C_{ex} = 1.3 \times 10^{-11}$ J/m. Typical values for the remaining physical constants are [8]: $j_e = 10^{11}$ A/m^2, $D_0 = 10^{-3}$ m^2/s for the magnetic layer, and $D_0 = 5 \times 10^{-3}$ m^2/s for the nonmagnetic layer, $\lambda_J = 4$ nm, $\lambda_{sf} = 10$ nm, $c = 3.125 \times 10^{-3}$ N/A^2, $\beta = 0.9$, $\beta' = 0.8$, and $\alpha = 0.1$. The current flows in the positive z direction. The simulations presented here were carried out using $\Delta z = 2$ nm, and $\Delta t = 10^{-12}$ s. No appreciable differences were found when smaller values of Δz or Δt were used. For the simulations presented here, formulas (9) and (10) were tested, with no appreciable difference in the results.

4.1. Reduction in the coercive field

We have considered a multilayer of in-plane dimensions 128 nm × 64 nm, and thicknesses $D_1 = 100$ nm, $D_2 = 20$ nm, and $D_3 = 60$ nm. We have computed the hysteresis loop with and without spin currents. The hysteresis loop is computed in the following way: Initially, an external field of magnitude h_0 is applied in order to saturate the sample, and the magnetization is allowed to reach equilibrium state. Once steady state is reached, the applied field is reduced, and the magnetization is allowed to reach equilibrium again. This process is repeated, decreasing the applied field each time by a fixed amount, until a negative field of magnitude h_0 is reached. In the hysteresis loop, we plot the average equilibrium magnetization as a function of the applied field. In our example, we consider $h_0 = 600$ Oe.

Typically, in a multilayer, the magnetization can be found in one of two states: The S state, and the C state, depicted schematically in Fig. 3. The magnetization reversal process associated to the S state usually

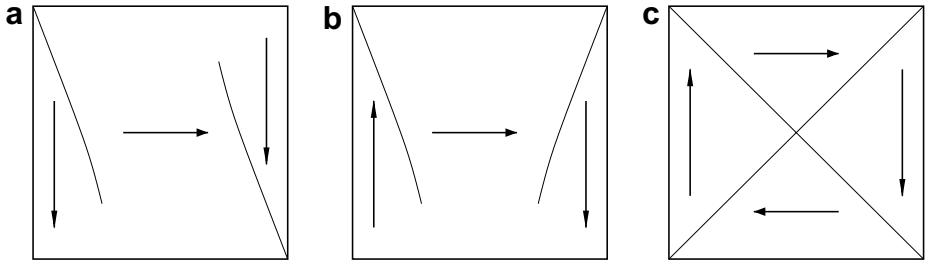

Fig. 3. Sketch of the (a) S state, (b) C state, and (c) Vortex state. The domain walls are depicted, and the arrows indicate the orientation of the magnetization.

occurs by a rotation of the magnetization in the interior of the domain, followed by the appearance of boundary layers, which can be removed if the applied field is strong enough. In the C state, the magnetization reversal process occurs by nucleating a magnetic vortex, which is subsequently expelled. Understanding the reversal process is of technological importance, given that if the boundary layers are not removed, or the vortex is not expelled, the information stored in the magnetic memory is essentially destroyed [18,13,12].

In Fig. (4) we have plotted the hysteresis loop associated with a double layer initialized with S states in each layer, and the loop associated with a double layer with C states in each layer. For the given dimensions, and in the absence of spin currents, a magnetic field of -600 Oe is not strong enough to switch the magnetization when both layers are in the S state. When both layers are in the C state, in the absence of spin currents, a vortex nucleates at approximately -260 Oe. A field of approximately -330 Oe is required to expel the vortex, and successfully reverse the magnetization.

When spin currents are present, the coercive field is reduced in both situations. The presence of a perpendicular current favors the nucleation of a magnetic vortex in the ferromagnetic sample, which has been found experimentally to reduce the coercive field [21]. In our simulation, the nucleation occurs at approximately -45 Oe, and the switching occurs at -250 Oe. In Fig. 5 we show the S state, and the intermediate vortex states that nucleates inside the sample during the reversal of the S state. For clarity of presentation, we plot only the in-plane components of the magnetization, at the center slice of the top layer.

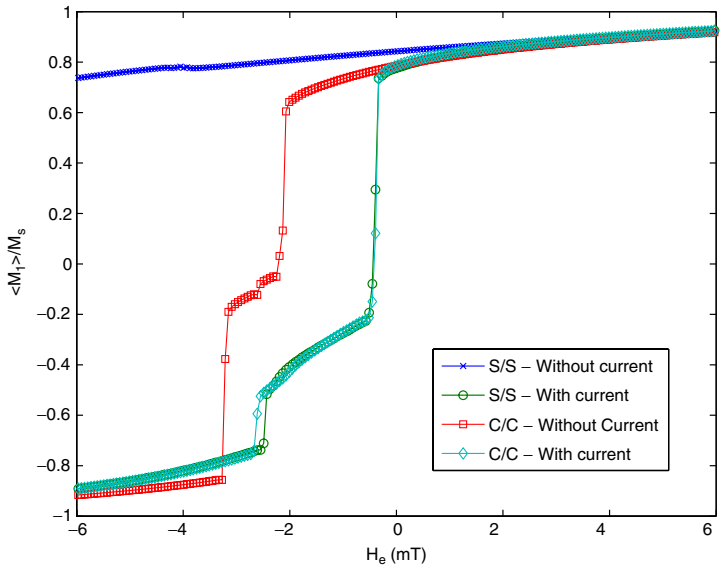

Fig. 4. Hysteresis loops for a multilayer with and without spin currents. The presence of spin currents lowers significantly the coercive field.

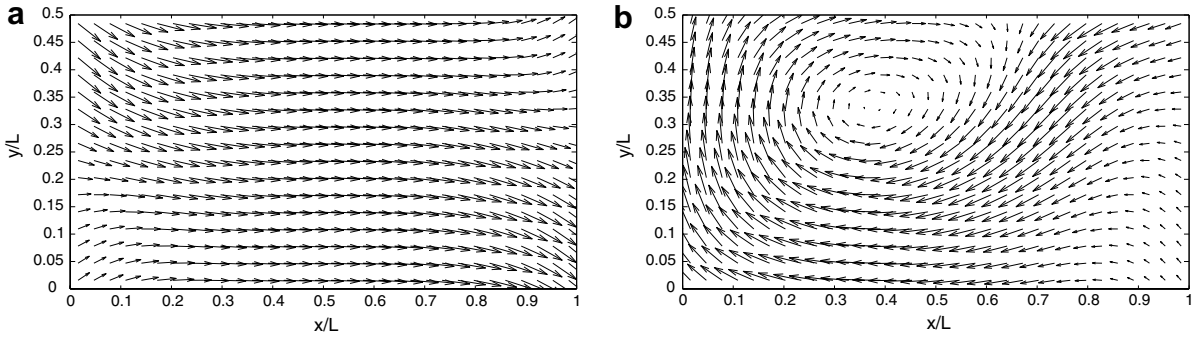

Fig. 5. States in the hysteresis loop: (a) S state, (b) nucleated vortex.

4.2. Current-driven magnetization reversal

One of the main technological applications of spin-polarized transport is the magnetization reversal in a multilayer in the absence of externally applied magnetic fields, as this can allow an increase in the density of magnetic memories. For this experiment, we have considered a multilayer with the same in-plane dimensions as before, but with thicknesses $D_1 = 200$ nm, $D_2 = 20$ nm, and $D_3 = 60$ nm. The multilayer was initialized in a uniform state, and it was allowed to reach steady state. Subsequently, a perpendicular current of magnitude $j_e = 10^{11}$ As was applied for 10 ns, and then it was removed. The average magnetization in the top layer is plotted in Fig. 6 as a function of time. The magnetization in the top layer was reversed as a consequence of the spin-currents, in agreement with recent experiments.

In conclusion, we have presented an implicit numerical method for the coupled system spin/magnetization in ferromagnetic multilayers. The complexity of the method is comparable with that of solving the linear heat equation with the Backward Euler method. Fully three dimensional simulations of the magnetization reversal process were carried out. In our experiments we have shown that the presence of spin-currents can significantly reduce the coercive field, by favoring the nucleation of magnetic vortices inside the ferromagnetic layer. In addition, we demonstrated that the spin current can induce the magnetization reversal process, even in the absence of externally applied magnetic fields.

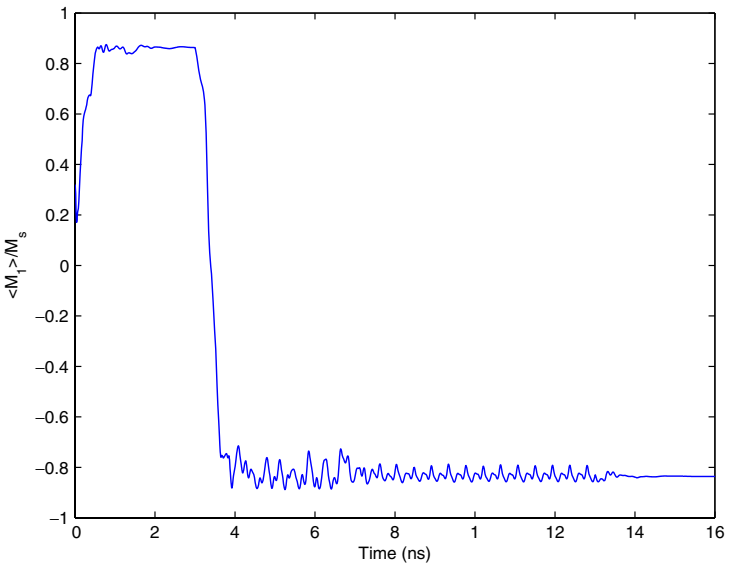

Fig. 6. Spin-current induced switching. The magnetic sample is saturated, and a perpendicular current flows through the multilayer, inducing the magnetization reversal process.

Acknowledgments

This work was initiated while García-Cervera was visiting the Mathematics Department at the Hong Kong University of Science and Technology. García-Cervera would like to thank everybody at the department for their hospitality. This work is partially supported by Hong Kong RGC-CERG Grant HKUST 603503P. The work of García-Cervera is also partially funded by NSF grant DMS-0505738, and a Faculty Career Development Award from UCSB. The work of Wang is also partially supported by RGC-CERG Grant HKUST 604105.

Appendix A. Gauss–Seidel projection method

For completeness, we include here a description of the GSPM, when spin currents are present. It is convenient to rewrite equation (3) in the following form:

$$\frac{\partial \mathbf{m}}{\partial t} = -\mathbf{m} \times (\epsilon \Delta \mathbf{m} + \mathbf{f}(\mathbf{m}, \mathbf{s})) - \alpha \mathbf{m} \times (\mathbf{m} \times (\epsilon \Delta \mathbf{m} + \mathbf{f}(\mathbf{m}, \mathbf{s}))), \tag{A.1}$$

where $\epsilon = 2C_{\text{ex}}\gamma/(M_{\text{s}}(1+\alpha^2))$, and

$$\mathbf{f}(\mathbf{m}, \mathbf{s}) = \frac{\gamma}{1+\alpha^2}\left(-\frac{2K_{\text{u}}}{M_{\text{s}}}(m_2\mathbf{e}_2 + m_3\mathbf{e}_3) + \mu_0(\mathbf{h}_{\text{s}} + \mathbf{h}_0) + c\mathbf{s}\right). \tag{A.2}$$

Eq. (A.1) is obtained by computing the vector product of $\mathbf{m}$ and Eq. (3), and solving for $\mathbf{m} \times \frac{\partial \mathbf{m}}{\partial t}$.

In the GSPM, we solve Eq. (A.1) in three steps:

Step 1. Implicit Gauss–Seidel.

$$\begin{aligned} g_i^n &= (I - \epsilon \Delta t \Delta_h)^{-1}(m_i^n + \Delta t f_i^n), \\ g_i^* &= (I - \epsilon \Delta t \Delta_h)^{-1}(m_i^* + \Delta t f_i^*), \qquad i = 1, 2, 3 \end{aligned} \tag{A.3}$$

$$\begin{pmatrix} m_1^* \\ m_2^* \\ m_3^* \end{pmatrix} = \begin{pmatrix} m_1^n + (g_2^n m_3^n - g_3^n m_2^n) \\ m_2^n + (g_3^n m_1^* - g_1^* m_3^n) \\ m_3^n + (g_1^* m_2^* - g_2^* m_1^*) \end{pmatrix}, \tag{A.4}$$

where $f_i^n = f_i(\mathbf{m}^n, \mathbf{s}^n)$, and $f_i^* = f_i(\mathbf{m}^*, \mathbf{s}^n)$, i.e., the most current values for $\mathbf{m}$ are used in $\mathbf{f}^*$. Note that the value of $\mathbf{s}$ is frozen at $t = t_n$.

Step 2. Heat flow without constraints.

$$\begin{pmatrix} m_1^{**} \\ m_2^{**} \\ m_3^{**} \end{pmatrix} = \begin{pmatrix} m_1^* + \alpha \Delta t(\epsilon \Delta_h m_1^{**} + f_1^*) \\ m_2^* + \alpha \Delta t(\epsilon \Delta_h m_2^{**} + f_2^*) \\ m_3^* + \alpha \Delta t(\epsilon \Delta_h m_3^{**} + f_3^*) \end{pmatrix}. \tag{A.5}$$

Step 3. Projection onto S^2.

$$\begin{pmatrix} m_1^{n+1} \\ m_2^{n+1} \\ m_3^{n+1} \end{pmatrix} = \frac{1}{|m^{**}|}\begin{pmatrix} m_1^{**} \\ m_2^{**} \\ m_3^{**} \end{pmatrix}. \tag{A.6}$$

References

[1] J.C. Slonczewski, Current-driven excitation of magnetic multilayers, J. Magn. Magn. Mat. 159 (1996) L1–L7.
[2] L. Berger, Emission of spin waves by a magnetic multilayer traversed by a current, Phys. Rev. B 54 (1996) 9353–9358.
[3] L. Berger, New origin for spin current and current-induced spin precession in magnetic multilayers, J. Appl. Phys. 89 (2001) 5521–5525.

[4] P.C. van Son, H. van Kempen, P. Wyder, Boundary resistance of the ferromagnetic-nonferromagnetic metal interface, Phys. Rev. Lett. 58 (1987) 2271–2273.
[5] M. Johnson, R.H. Silsbee, Coupling of electronic charge and spin at a ferromagnetic-paramagnetic metal interface, Phys. Rev. B 37 (1988) 5312–5325.
[6] T. Valet, A. Fert, Theory of the perpendicular magnetoresistance in magnetic multilayers, Phys. Rev. B 48 (1993) 7099–7113.
[7] S. Zhang, P.M. Levy, A. Fert, Mechanisms of spin-polarized current-driven magnetication switching, Phys. Rev. Lett. 88 (2002) 236601.
[8] A. Shpiro, P.M. Levy, S. Zhang, Self-consistent treatment of nonequilibrium spin torques in magnetic multilayers, Phys. Rev. B 67 (2003) 104430.
[9] C.J. García-Cervera, X.P. Wang, Spin-polarized transport: existence of weak solutions, Disc. Cont. Dyn. Sys. Series B 7 (1) (2005) 87–100.
[10] L. Landau, E. Lifshitz, On the theory of the dispersion of magnetic permeability in ferromagnetic bodies, Physikalische Zeitschrift der Sowjetunion 8 (1935) 153–169.
[11] T.L. Gilbert. Phys. Rev., 100:1243, 1955. [Abstract only; full report, Armor Research Foundation Project No. A059, Supplementary Report, May 1, 1956] (unpublished).
[12] J. Shi, T. Zhu, S. Tehrani, Y.F. Zheng, J.-G. Zhu, Magnetization vortices and anomalous switching in patterned NiFeCo submicron arrays, Appl. Phys. Lett. 74 (1999) 2525–2527.
[13] A.F. Popkov, L.L. Savchenko, N.V. Vorotnikova, S. Tehrani, J. Shi, Edge pinning effect in single- and three-layer patterns, Appl. Phys. Lett. 77 (2) (2000) 277–279.
[14] J.D. Lambert, Computational Methods in Ordinary Differential Equations, John Wiley & Sons, London-New York-Sydney, 1973, Introductory Mathematics for Scientists and Engineers.
[15] D. Lewis, N. Nigam, Geometric integration on spheres and some interesting applications, J. Comput. Appl. Math. 151 (1) (2003) 141–170.
[16] Jason Frank, Geometric space-time integration of ferromagnetic materials, in: Workshop on Innovative Time Integrators for PDEs, Appl. Numer. Math. 48 (3–4) (2004) 307–322.
[17] Y. Nakatani, Y. Uesake, N. Hayashi, Direct solution of the Landau–Lifshitz–Gilbert equation for micromagnetics, Japanese Journal of Applied Physics 28 (12) (1989) 2485–2507.
[18] C. García-Cervera, X.-P. Wang, W. E, A Gauss–Seidel projection method for micromagnetics simulations, J. Comp. Phys. 171 (2001) 357–372.
[19] C. García-Cervera, W. E, Improved Gauss-Seidel projection method for micromagnetics simulations, IEEE Transactions on Magnetics 39 (3) (2003) 1766–1770.
[20] C.J. García-Cervera, Z. Gimbutas, W. E, Accurate numerical methods for micromagnetics simulations with general geometries, J. Comp. Phys. 184 (1) (2003) 37–52.
[21] K.J. Kirk, M.R. Scheinfein, J.N. Chapman, S. McVitie, M.F. Gillies, B.R. Ward, J.G. Tennant, Role of vortices in magnetization reversal of rectangular NiFe elements, J. Phys. D: Appl. Phys. 34 (2001) 160–166.